Single-particle and collective properties of drip-line nuclei

I. Hamamoto,[1] H. Sagawa,[1,2] and X. Z. Zhang[1,3]
[1]*Department of Mathematical Physics, Lund Institute of Technology at University of Lund, Lund, Sweden*
[2]*Center for Mathematical Sciences, University of Aizu, Ikki-machi, Aizu-Wakamatsu, Fukushima 965, Japan*
[3]*Institute of Atomic Energy, Beijing, The People's Republic of China*
(Received 10 October 1995)

We study the effect of the unique shell structure as well as the very low particle threshold on collective modes in drip-line nuclei, first performing the Hartree-Fock (HF) calculation with Skyrme interactions and, then, using the random phase approximation solved in the coordinate space with the Green's function method. We examine also one-particle resonant states in the HF potential. The properties of both isoscalar and isovector monopole giant resonance (GR) are found to change drastically in nuclei around the neutron drip line. The characteristic feature of the isovector dipole modes as well as the isoscalar quadrupole modes in drip-line nuclei is also studied.

PACS number(s): 21.10.Pc, 21.10.Re, 21.60.Jz, 27.60.+j

I. INTRODUCTION

Using radioactive nuclear beams being recently developed at various laboratories in the world [1] we have a good prospect to investigate the detailed structure of nuclei far from β stability. The investigations also involve strong links between nuclear physics and astrophysics. Thus, it is currently a very hot issue to find the phenomena unique in nuclei far from β stability, which are drastically different from those in β-stable nuclei. The neutron halo at the neutron drip line [2] of very light nuclei is a typical example of that kind, which is found and studied both experimentally and theoretically. The variation of the one-particle level structure as one approaches the drip line has been studied for spherical nuclei, using a relativistic mean-field approach [3] and an HFB approach [4]. The possible presence of a neutron skin in neutron-rich nuclei near the neutron drip line has also been studied and discussed in the literature [5,6]. Using deformed HF calculations, in Ref. [7] a series of medium-heavy neutron-rich nuclei is found, in which the presence of the neutron skin can be recognized and yet the neutron one-particle spectra are far from those in a harmonic oscillator (plus spin-orbit) potential. The conclusion of Ref. [7] is drawn from the study of one-particle levels which are bound by more than 1 MeV.

In this paper we aim at the investigation of the single-particle and the collective properties unique in drip-line nuclei by focusing our attention to the shell structure embedded in the continuum. First, performing the calculation of one-particle resonant states [8] in the HF potential, we study the variation of one-particle spectra of spherical nuclei for a given mass number going from the proton drip line to the neutron drip line. Analyzing the obtained one-particle spectra in terms of the l^2 term used in the modified oscillator potential we try to parametrize the quantitative information on the variation of the HF potential. We examine also directly the calculated proton and neutron densities as well as the variation of the radial shape of the HF potential. Second, we estimate collective properties of the nuclei, using the RPA with the same Skyrme interaction as used in the HF calculation and with the Green's function method [9] which produces a proper strength function in the continuum. All basic information on the shell structure, which affects the collective modes, is indeed obtained from a careful examination of the unperturbed strength function. Both isoscalar and isovector monopole modes are first studied in detail, since in a simple-minded picture only one peak is expected for the monopole giant resonance (GR). Moreover, the properties of monopole modes are especially sensitive to the detailed balance between the density distributions of the inside and around the surface. Next, we examine the properties of isovector dipole modes and isoscalar quadrupole modes in nuclei at both the proton drip line and the neutron drip line, and compare them with those known in β-stable nuclei.

Our present work is based on the spherical HF calculation with Skyrme interactions. The parameters of the effective interactions such as Skyrme interactions are determined so as to reproduce the known properties of β-stable nuclei. Therefore, Skyrme interactions with different parameters may produce different properties for nuclei far from the β-stability line. In this paper we use the SkM* interaction as a standard Skyrme interaction, however, we always check whether or not the same conclusion can be drawn when we use other Skyrme interactions. As numerical examples we choose nuclei with the mass number $A \approx 120$, which are large enough to obtain a variety of one-particle j shells around the Fermi level.

In Sec. II the result of single-particle properties obtained from the calculation of the HF and one-particle resonant states is presented and discussed. In Sec. III the result of collective (isoscalar monopole, isovector monopole, isovector dipole, and isoscalar quadrupole) modes is given and discussed. Conclusions and further discussions are presented in Sec. IV.

II. SINGLE-PARTICLE PROPERTIES

The HF equation for spherical shape is solved by the Numerov algorithm with a space mesh size 0.1 fm and 200 mesh points. Then, the reference radius R of the calculations is 20 fm, which is large enough for the drip-line nuclei studied in our present work. The one-particle levels are filled from the lowest one upward. For open-shell nuclei the last-

occupied j shell is partially filled. If configurations, among which the partially filled j shell is different, will energetically compete, we choose the configuration which has the lowest total energy calculated in the HF approach.

After having fixed the HF configuration, unoccupied one-particle levels are calculated for the HF potential. Eigenvalues of one-particle levels with negative energies can be easily obtained with good accuracy. We estimate all one-particle levels belonging to one major shell above the Fermi level. If those levels lie in the continuum we try to evaluate one-particle resonance energies. The resonant states are found so that the phase shift passes through $\pi/2$ with positive slope at the one-particle energies. It is easy to obtain the resonant states for protons, because of the presence of an appreciably high Coulomb barrier outside of the nuclei. In contrast, for the neutron one-particle states with lower orbital angular-momenta the resonant states are not always obtained because of the lack of a sufficiently high centrifugal barrier.

In Figs. 1(a) and 1(b) we show the calculated neutron one-particle spectra for the mass number, $A=120$ and $A=110$, respectively, going from the proton drip line to the neutron drip line, while in Fig. 2 the corresponding proton one-particle spectra for $A=120$ are plotted. For the one-particle levels with positive energies the solid circles show the calculated energies of resonant states, while the absence of solid circles in Fig. 1 indicate that resonant states are not obtained. In the latter case we have taken a procedure of estimating the energies by adjusting reference radius R of the HF equation so that the resulting one-particle energies become a smooth continuation of the bound (or resonant) energies obtained for smaller neutron numbers. Although this procedure is not mathematically founded we expect to obtain a reasonable idea of the energy values. From Fig. 1 it is clearly observed that among neutron one-particle levels close to zero energies the levels with lower orbital angular momenta are pushed down relative to those with higher angular momenta, as the neutron drip line approaches. We observe a similar, but much less pronounced, tendency in some proton resonant energies in Fig. 2, as we approach the proton drip line. Furthermore, it is seen in Fig. 1 that as we approach the neutron drip line the energies of some neutron particle-hole (p-h) excitations across the major shell will become considerably smaller. The influence of the smaller energies on the properties of collective modes will be studied in Sec. III, treating particles in the continuum in a proper way.

Analyzing the calculated one-particle energies in terms of the l^2 term used in the modified oscillator potential (for example, see Ref. [10]) we try to quantify the observation described in the previous paragraph. The l^2 term was added to the oscillator potential so as to lower one-particle energies with larger l relative to those with smaller l, corresponding to the single-particle level ordering in the potential with a surface. In Fig. 3 we plot the quantity [4]

$$\varepsilon_l - \varepsilon_{l_{\min}}, \tag{1}$$

where $l_{\min}$ is equal to 0 for $N_{sh}[\equiv 2(n-1)+l]$=even and 1 for N_{sh}=odd. The quantity

$$\varepsilon_l = \frac{1}{2l+1}\left[l\varepsilon_{j=l+1/2}+(l+1)\varepsilon_{j=l-1/2}\right] \tag{2}$$

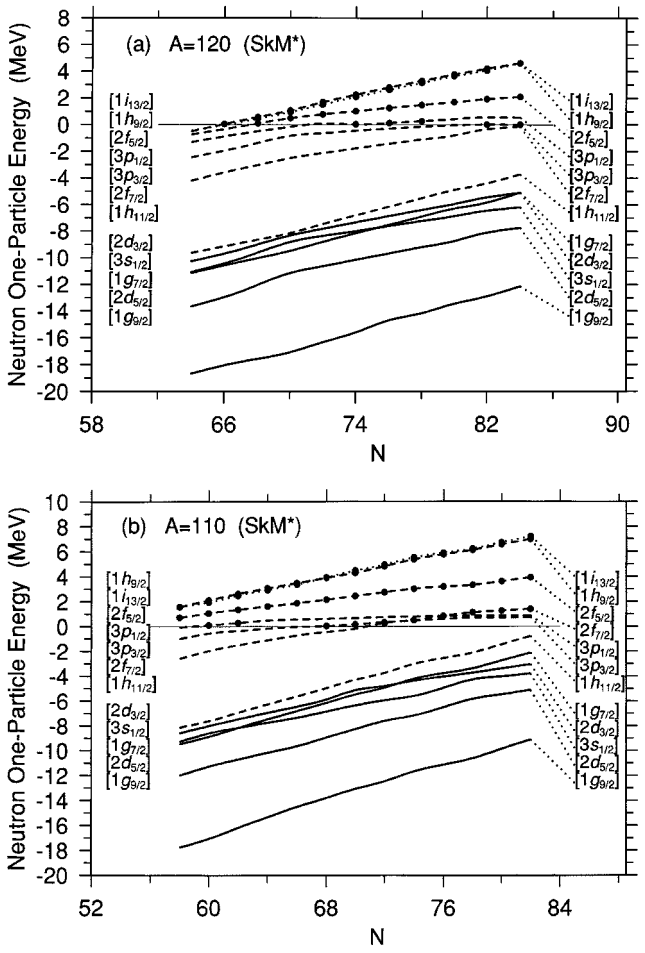

FIG. 1. Neutron one-particle spectra for nuclei with a fixed mass number as a function of neutron number: (a) $A=120$ and (b) $A=110$. For a given A the energy levels are calculated for all even-even nuclei from the proton drip line to the neutron drip line. The solid circles with positive energies are obtained as one-particle resonant states. The levels of a given j shell with $N_{sh}[\equiv 2(n-1)+l]=4$ are connected by solid lines, those with $N_{sh}=5$ by dashed lines, and those with $N_{sh}=6$ by dotted lines. On the left side of the figure the quantum numbers $[nl_j]$ of the levels are denoted according to the energy order. On the right-hand side the quantum numbers are given in the same way, with an explicit indication by dotted lines.

expresses the one-particle energy averaged over spin-orbit partners with the orbital angular momentum l. The values of (1) are calculated using energies in Fig. 1 for a given value of N_{sh} as a function of orbital angular momenta of neutrons. Solid circles and squares connected by solid lines denote the quantity in (1) for β-stable nuclei, while unfilled signs connected with dashed lines are for neutron-drip-line nuclei. From Fig. 3 it is seen that the coefficient of the l^2 term in the neutron-drip-line nuclei becomes zero or obtains even an opposite sign for the partially filled $N_{sh}=5$ major shell. An opposite sign of the l^2 term means that, compared with the harmonic oscillator spectra, one-particle orbitals with lower angular momenta and more radial nodes are energetically pushed down relative to those with higher angular momenta and less radial nodes. The pushing down is a result of the HF potential with a very diffused surface. This change of the l^2 term is very pronounced only for the levels with $\varepsilon \gtrsim -1.5$

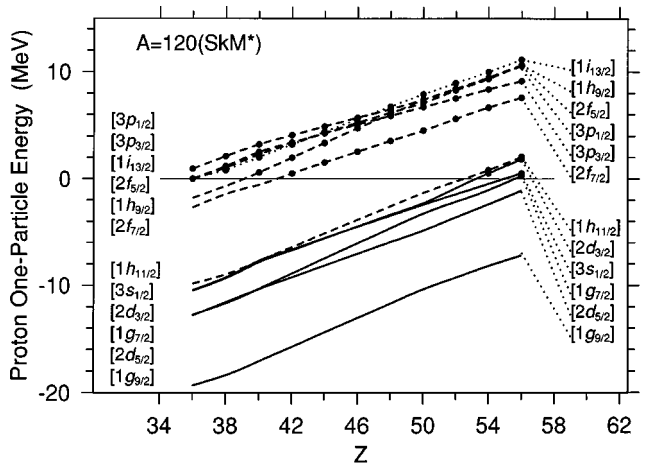

FIG. 2. Proton one-particle spectra for $A=120$ as a function of proton number, from the neutron drip line to the proton drip line. See caption to Fig. 1.

MeV, as seen in Fig. 3. The quantity in (1) for the deeply bound neutron orbitals in the neutron-drip-line nuclei is not so different from that in the β-stable nuclei.

Using only bound one-particle levels calculated with the SkP interaction, a similar result of the l^2 term for the case of $N_{sh}=4$ and $l=4$ is previously pointed out in Ref. [4]. If we draw Fig. 1(a) using the SkP interaction, which will be the same figure as a part of Fig. 3 of Ref. [4] except the part for positive energies, our conclusion remains semiquantitatively the same. The only noticeable difference is that in the case of the SkP interaction all energy levels below the neutron number $N=82$ are appreciably pushed up in all nuclei. That means, the $N=82$ shell gap (namely, the energy distance between the $1h_{11/2}$ level and other $N_{sh}=5$ levels) becomes, as a total, appreciably smaller for the SkP interaction. The smaller shell gap may lead to a considerably different result in astrophysical r process [11].

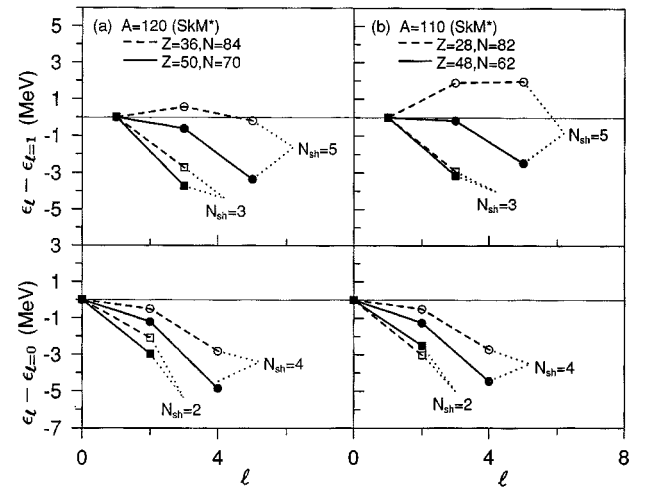

FIG. 3. Evaluation of the l^2 term in neutron one-particle spectra; $\varepsilon_l-\varepsilon_{l\min}$ in Eq. (1) is plotted as a function of orbital angular momentum. The left half of the figure is for $A=120$, while the right half for $A=110$. Unfilled marks connected by dashed lines denote the quantity for neutron-drip-line nuclei, while filled marks connected by solid lines express that for β-stable nuclei.

TABLE I. Mean energy distance between the N_{sh} shell and the $N_{sh}-2$ shell estimated for three $A=120$ nuclei; the neutron-drip-line nucleus $^{120}_{36}\mathrm{Kr}_{84}$, the β-stable nucleus $^{120}_{50}\mathrm{Sn}_{70}$, and the proton-drip-line nucleus $^{120}_{56}\mathrm{Ba}_{64}$. $\varepsilon_{N_{sh}}$ is defined in Eq. (3).

		$Z=36$ $N=84$	$Z=50$ $N=70$	$Z=56$ $N=64$
n	$\varepsilon_{N_{sh}=5}-\varepsilon_{N_{sh}=3}$ (MeV)	17.9	19.7	20.2
n	$\varepsilon_{N_{sh}=4}-\varepsilon_{N_{sh}=2}$ (MeV)	19.2	20.1	20.2
p	$\varepsilon_{N_{sh}=4}-\varepsilon_{N_{sh}=2}$ (MeV)	20.8	20.4	20.1

From energies in Figs. 1 and 2 we extract the quantity

$$\varepsilon_{N_{sh}}=\frac{\Sigma_j^{(N_{sh})}(2j+1)\varepsilon_j}{\Sigma_j^{(N_{sh})}(2j+1)}. \tag{3}$$

In Table I we show the calculated values of $\varepsilon_{N_{sh}}-\varepsilon_{N_{sh}-2}$ for three $A=120$ nuclei; the neutron-drip-line nucleus $^{120}_{36}\mathrm{Kr}_{84}$ and the β-stable nucleus $^{120}_{50}\mathrm{Sn}_{70}$ and the proton-drip-line nucleus $^{120}_{56}\mathrm{Ba}_{64}$. We observe that the mean energy distance between neutron major shells decreases appreciably around the Fermi surface of neutron-drip-line nuclei. A detailed study shows that one-particle one-hole (1p-1h) $\Delta N_{sh}=2$ excitations with smaller j values have much smaller excitation energies than the values given in Table I. Furthermore, the results in Table I suggests that if we could have estimated the value of $\varepsilon_{N_{sh}=6}-\varepsilon_{N_{sh}=4}$ for neutrons in $^{120}_{36}\mathrm{Kr}_{84}$ it would have been much smaller than 17 MeV. The small energies of the neutron 1p-1h $\Delta N_{sh}=2$ excitations, in which the holes are in the last filled shells of the doubly magic neutron-drip-line nucleus $^{110}_{28}\mathrm{Ni}_{82}$, are carefully studied in Sec. III A in connection with the isoscalar monopole mode.

In order to exhibit the presence of the neutron skin in neutron-drip-line nuclei considered presently, in Fig. 4(a) we show the HF density as well as the neutron HF potential for two extreme nuclei, the proton-drip-line nucleus $^{100}_{50}\mathrm{Sn}_{50}$ and the neutron-drip-line nucleus $^{110}_{28}\mathrm{Ni}_{82}$, which have the spherical shape in the ground states. In Fig. 4(b) we show the same quantities for two $A=120$ nuclei, the nucleus $^{120}_{38}\mathrm{Sr}_{82}$ lying close to the neutron drip line and the β-stable nucleus $^{120}_{50}\mathrm{Sn}_{70}$. In Sec. III those nuclei in Fig. 4 are used as examples for illustrating the calculated properties of collective modes. From the upper part of Figs. 4(a) and 4(b) the presence of the neutron skin is clearly seen for the nuclei $^{110}_{28}\mathrm{Ni}_{82}$ and $^{120}_{38}\mathrm{Sr}_{82}$. In the lower part of Fig. 4(a) the very diffused surface of the neutron potential of $^{110}_{28}\mathrm{Ni}_{82}$ is demonstrated, in contrast to the shape of the neutron potential of $^{100}_{50}\mathrm{Sn}_{50}$. The considerably deeper depth of V_n for $^{100}_{50}\mathrm{Sn}_{50}$ than for $^{110}_{28}\mathrm{Ni}_{82}$ is known to come from the larger proton number and the strongly attractive neutron-proton interaction. Since in $^{100}_{50}\mathrm{Sn}_{50}$ the energy of the last filled level of protons is only 3.2 MeV compared with 17.0 MeV of neutrons, in the upper part of Fig. 4(a) it is seen that the proton density is larger than the neutron density outside of the nuclear surface, in spite of the presence of the large Coulomb barrier for protons.

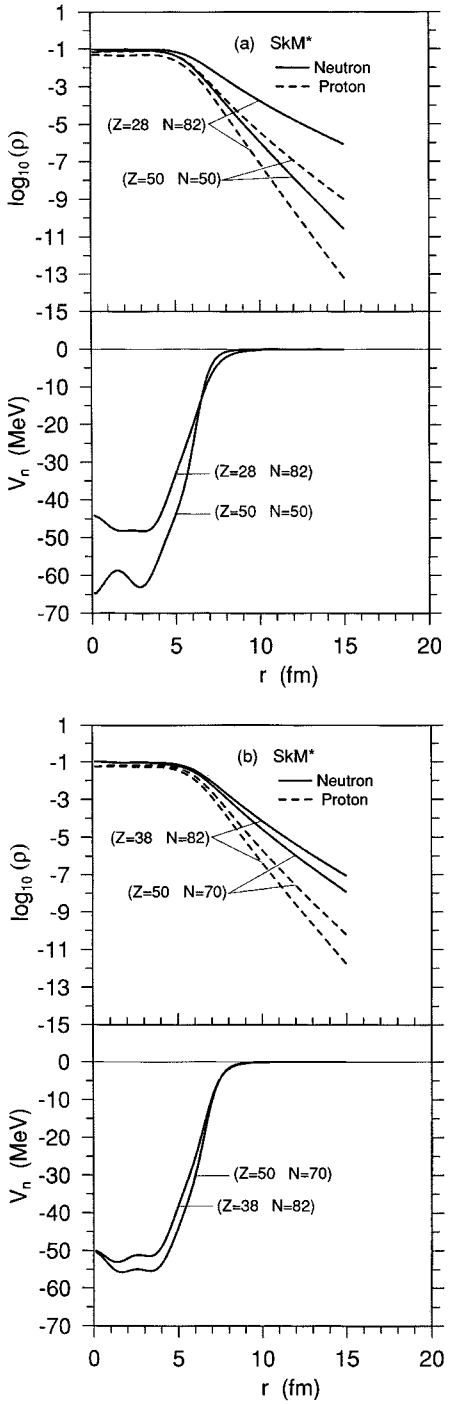

FIG. 4. Calculated HF density and neutron HF potential as a function of radial coordinate: (a) $^{110}_{28}\mathrm{Ni}_{82}$ and $^{100}_{50}\mathrm{Sn}_{50}$; (b) two $A=120$ nuclei, $^{120}_{38}\mathrm{Sr}_{82}$ and $^{120}_{50}\mathrm{Sn}_{70}$. The density ρ expressed in the unit of fm^{-3} is plotted in the logarithmic scale.

III. COLLECTIVE MODES

Using the same Skyrme interaction as used in the HF calculation, collective modes are calculated in the RPA with the Green's function technique solved in the coordinate space [12]. Spherical nuclei, in which the pair correlation will not play a role, are considered in the following. We examine both the unperturbed strength function

$$S_0(E)\equiv\sum_i |\langle i|Q|0\rangle|^2\delta(E-E_i)$$

$$=\frac{1}{\pi}\,\mathrm{Im\ Tr}[Q^\dagger G_0(E)Q], \tag{4}$$

where G_0 is the noninteracting p-h Green function, and the RPA strength function

$$S(E)\equiv\sum_n |\langle n|Q|0\rangle|^2\delta(E-E_n)$$

$$=\frac{1}{\pi}\,\mathrm{Im\ Tr}[Q^\dagger G_{\mathrm{RPA}}(E)Q]. \tag{5}$$

In Eqs. (4) and (5) Q expresses one-body operators, which are written as

$$Q^{\lambda=0,\tau=0}=\sum_i r_i^2 Y_{00}(\hat{r}_i)$$

for isoscalar monopole modes, (6)

$$Q^{\lambda=0,\tau=1}=\sum_i \tau_z r_i^2 Y_{00}(\hat{r}_i)$$

for isovector monopole modes, (7)

$$Q_\mu^{\lambda=2,\tau=0}=\sum_i r_i^2 Y_{2\mu}(\hat{r}_i)$$

for isoscalar quadrupole modes, and (8)

$$Q_\mu^{\lambda=1,\tau=1}=\sum_i \tau_z r_i Y_{1\mu}(\hat{r}_i)$$

for isovector dipole modes. (9)

For bound states below the particle threshold the excitation energies and the transition strengths appear as poles and residues, respectively, of the real part of the response functions $\mathrm{Tr}(Q^\dagger G_{\mathrm{RPA}}Q)$. Thus, they have to be found in a different way from calculating the expression in (5). From the same mathematical reason, the unperturbed strength function defined in Eq. (4) does not contain the strength of the bound p-h excitations, in which the particle occupies a bound one-particle state. However, if the unperturbed energies of those p-h excitations are above the particle threshold, the strength of those p-h excitations appears in the calculated RPA strength function in (5), due to the coupling to the continuum. We note that in neutron (proton)-drip-line nuclei the proton (neutron) potential is so deep that the major part of proton (neutron) p-h excitations, in which proton (neutron) particles are in bound one-particle states, can easily lie above the particle threshold. In any case we always check the energy-weighted sum rule, in order to make sure that an appreciable strength is not missing in our RPA strength functions.

In the present calculation the particle escape width is fully included, since we treat the particle continuum in a proper

way. However, the spreading width of collective modes due to the coupling to nearby complicated (many-particle–many-hole) configurations are not included.

The transition density for an excited state $|n\rangle$,

$$\rho^{\rm tr}_{n0}(\mathbf{r}) \equiv \left\langle n \left| \sum_{i=1}^{A} \delta(\mathbf{r}-\mathbf{r}_i) \right| 0 \right\rangle \tag{10}$$

can also be calculated, since the imaginary (real) part of $G_{\rm RPA}(\mathbf{r},\mathbf{r}';E_n)$ is proportional to $\rho^{\rm tr}_{n0}(\mathbf{r})\rho^{\rm tr}_{n0}(\mathbf{r}')^{\dagger}$ when E_n is above (below) the particle threshold. Using the transition density in Eq. (10) one obtains the reduced transition probability

$$B(\lambda,\tau{:}0\rightarrow n) = \sum_{\mu} \left| \int \rho^{\rm tr}_{n0}(\mathbf{r}) Q^{\lambda\tau}_{\mu}\, d^3r \right|^2, \tag{11}$$

where the excited state denoted by n has the angular momentum $(\lambda\mu)$. The radial transition density $\rho^{\rm tr}_{\lambda}(r)$ is defined by

$$\rho^{\rm tr}_{n0}(\mathbf{r}) \equiv \rho^{\rm tr}_{\lambda}(r) Y_{\lambda\mu}(\hat{r}). \tag{12}$$

It is useful to estimate the moments m_k defined by

$$m_k \equiv \sum_n (E_n - E_0)^k |\langle n|Q|0\rangle|^2. \tag{13}$$

Defining the various mean energies $\bar{E}_k$ by

$$\bar{E}_k = \sqrt{\frac{m_k}{m_{k-2}}}, \tag{14}$$

$\bar{E}_1$ and $\bar{E}_3$ are often used, which are equal to each other if the system has only one sharp peak excited by the operator Q. The difference between the values of E_1 and E_3 expresses a measure of the width or the degree of the fragmentation of the strength.

As numerical examples to illustrate the dynamics unique in drip-line nuclei we choose two doubly magic nuclei $^{100}_{50}\mathrm{Sn}_{50}$ and $^{110}_{28}\mathrm{Ni}_{82}$ at the proton drip line and the neutron drip line, respectively. The nucleus $^{100}_{50}\mathrm{Sn}_{50}$ was recently found and some experimental spectroscopic information may soon be obtained. On the other hand, it may take years to make the nucleus $^{110}_{28}\mathrm{Ni}_{82}$. For comparison we present also some numerical results of two $A=120$ nuclei, the β-stable nucleus $^{120}_{50}\mathrm{Sn}_{70}$ and the nucleus $^{120}_{38}\mathrm{Sr}_{82}$ which lies closely to the neutron drip line.

A. Isoscalar and isovector monopole modes

In Fig. 5 we show the unperturbed strength function in Eq. (4) as well as the RPA strength function in Eq. (5) for the isoscalar and the isovector monopole modes. Already when we compare the unperturbed strength function of $^{110}_{28}\mathrm{Ni}_{82}$ in Fig. 5(a) with that of $^{100}_{50}\mathrm{Sn}_{50}$ in Fig. 5(b), a clear difference is seen. In $^{110}_{28}\mathrm{Ni}_{82}$ the particle threshold is 0.8 MeV [see Fig. 1(b)], which is the energy required for one neutron in the last filled $1h_{11/2}$ shell to be excited into the continuum. However, the strength [i.e., the dotted line in Fig. 5(a)] begins to rise steeply [13,14] first around 3.8 MeV, which is equal to the energy required for one neutron in the occupied $3s_{1/2}$ shell to be excited into ($s_{1/2}$ states in) the continuum. The major part of the unperturbed neutron strength of the monopole operator in expression (6) [or (7)] is found below 20 MeV. A detailed study of the strength expressed by the dotted line in Fig. 5(a) shows

(a) for the configurations with the neutron hole in the $1h_{11/2}$, $1g_{7/2}$, $2d_{3/2}$, $3s_{1/2}$, and $2d_{5/2}$ shells (i.e., the last-filled major shell) the monopole strength starts to appear at the excitation energy of 0.8–5.1 MeV and reaches the maximum at 6–10 MeV, having a large tail on the higher-energy side. For example, the strength with the hole in the $1h_{11/2}$ shell starts at 0.8 MeV and reaches the maximum around 10 MeV, while the one in the $3s_{1/2}$-shell begins at 3.8 MeV with the maximum at 6.3 MeV. The energies of those maxima have nothing to do with the one-particle resonance energies [15] and, indeed, no resonant states with the respective quantum numbers l_j are found in this nucleus ^{110}Ni;

(b) for the holes in the $1g_{9/2}$, $2p_{1/2}$, $1f_{5/2}$, and $2p_{3/2}$ shells (i.e., the major shell for $28<N\leqslant 50$) the strength starts at 9.1–13.0 MeV with the peaks at 12–16 MeV;

(c) for the holes in the $1f_{7/2}$ shell (i.e., the shell for $20<N\leqslant 28$) the strength starts at 17.5 MeV and has a peak at $E_x\sim 18.7$ MeV, which is the relatively narrow peak seen in the dotted line of Fig. 5(a). The peak energy is nearly equal to the energy of the $1f_{7/2}\rightarrow$(resonant)$2f_{7/2}$ excitation.

The above results (a)–(c) explain the peaks of the unperturbed neutron strength in Fig. 5(a), dividing the excitation energy into the three regions, 6–10, 12–16, and ~18.7 MeV. It is remarkable to see that a significant part of the unperturbed monopole strengths, which lie at the frequency of $2\hbar\omega_0$ ($=17$ MeV for $A=110$) in the harmonic oscillator model, appears at so low excitation energies. In contrast, there is no unperturbed proton strength below 22 MeV, and the bound proton p-h excitations, $1p_{3/2}\rightarrow 2p_{3/2}$, $1p_{1/2}\rightarrow 2p_{1/2}$, $2s_{1/2}\rightarrow 3s_{1/2}$, $1d_{3/2}\rightarrow 2d_{3/2}$, $1d_{5/2}\rightarrow 2d_{5/2}$, and $1f_{7/2}\rightarrow 2f_{7/2}$, lie at $E_x=22.2$–26.2 MeV. Examining the plotted RPA solution for both isoscalar and isovector modes, we see that those bound proton p-h excitations couple weakly with the excitations in the continuum and some part of the p-h strengths remains nearly at the same energy region after solving RPA. This weak coupling of some p-h configurations is a feature of the monopole mode, of which the coupling has not only a peak at the surface but also an important contribution from the inside of the nucleus that can cancel the surface-peak contribution.

In $^{100}_{50}\mathrm{Sn}_{50}$ the particle (proton) threshold is at 3.2 MeV, however, an appreciable unperturbed strength starts to appear first around 12 MeV because of the presence of the large Coulomb barrier. Thus, the unperturbed strength in (4) is concentrated in a relatively narrow energy region centered around 22 MeV. All unperturbed proton strength is included in the dotted line of Fig. 5(b). On the other hand, since the neutron threshold of $^{100}_{50}\mathrm{Sn}_{50}$ is 17.0 MeV, there are bound neutron p-h excitations, which do not appear in dotted lines of Fig. 5(b). They are $2s_{1/2}\rightarrow 3s_{1/2}$ at 22.2 MeV, $1d_{3/2}\rightarrow 2d_{3/2}$ at 24.3 MeV, $1d_{5/2}\rightarrow 2d_{5/2}$ at 24.8 MeV, and $1f_{7/2}\rightarrow 2f_{7/2}$ at 25.2 MeV. These energies are very similar to those of the unperturbed proton excitations, in contrast to the case of $^{110}_{28}\mathrm{Ni}_{82}$.

The difference between the properties of the RPA monopole modes of ^{110}Ni and those of ^{100}Sn is very prominent. In

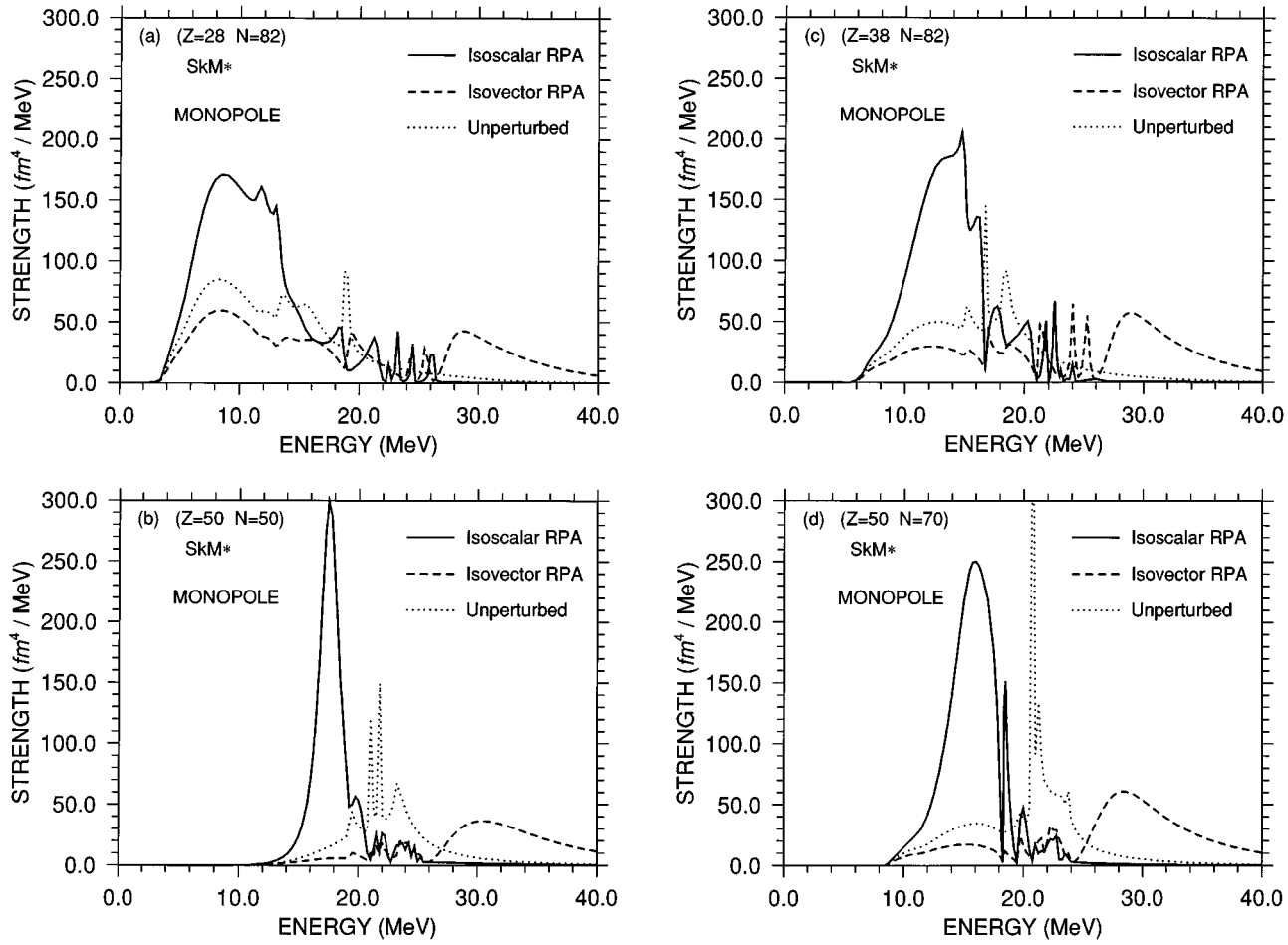

FIG. 5. The unperturbed strength function defined in Eq. (4) and the RPA strength function in Eq. (5) for isoscalar and isovector monopole modes as a function of excitation energy: (a) $^{110}_{28}Ni_{82}$, (b) $^{100}_{50}Sn_{50}$, (c) $^{120}_{38}Sr_{82}$, and (d) $^{120}_{50}Sn_{70}$. The unperturbed strength function is the same for the isoscalar and the isovector operators. In the region of 20–26 MeV several bound p-h excitations (proton configurations for ^{110}Ni and neutron configurations for ^{100}Sn) are present, which do not appear in the dotted lines of the figures. However, the presence of those p-h excitations can be recognized as peaks seen in the RPA strength function. See the text for details.

$^{110}_{28}Ni_{82}$ the major part of the isoscalar strength is shifted to the region of a very low excitation energy and the GR obtains a very broad width. Both the very low frequency and the broad width of the GR are the direct result of the characteristic feature of the unperturbed strength distribution in the neutron-drip-line nucleus, which is described above in detail. In contrast, the RPA strength of $^{100}_{50}Sn_{50}$ is concentrated nearly to one GR peak with a relatively narrow width. The properties of the RPA isoscalar GR in $^{100}_{50}Sn_{50}$ are in fact rather similar to those known in β-stable nuclei.

The RPA isovector strength in $^{110}_{28}Ni_{82}$ shows an extremely broad distribution and consists of, roughly speaking, two parts; the lower part coming exclusively from the neutron strength in which neutron holes are in the last-filled major shells and the higher peak which is analogous to the isovector GR known in β-stable nuclei. In contrast, the RPA isovector strength of $^{100}_{50}Sn_{50}$ has only one isovector GR peak similar to the one in β-stable nuclei, though some strength can be found in the lower-energy region.

The main features of monopole modes in $^{100}_{50}Sn_{50}$ are rather similar to those in β-stable nuclei, while monopole modes in $^{110}_{28}Ni_{82}$ show drastically different properties. In order to further illustrate this similarity and difference, in Figs. 5(c) and 5(d) we show the calculated result of two $A=120$ nuclei, $^{120}_{38}Sr_{82}$ lying close to the neutron drip line and $^{120}_{50}Sn_{70}$ being β stable. It is seen that monopole modes in $^{120}_{38}Sr_{82}$ ($^{120}_{50}Sn_{70}$) exhibit the characteristic features seen in $^{110}_{28}Ni_{82}$ ($^{100}_{50}Sn_{50}$), but not in a so extreme way as shown in Fig. 5(a) [5(b)]. The particle (neutron) threshold energy in $^{120}_{38}Sr_{82}$ is 4.4 MeV [see Fig. 1(a)]. However, the strength [i.e., the dotted line in Fig. 5(c)] starts to rise steeply first around 6.5 MeV, which is the energy required for one neutron in the $3s_{1/2}$ shell to be excited into the continuum. Comparing Fig. 5(c) with Fig. 5(d) we find it remarkable that the shape of the calculated isovector GR, which has a peak around 29 MeV and a large tail on the higher-energy side, is nearly identical in $^{120}_{38}Sr_{82}$ and $^{120}_{50}Sn_{70}$ for $E>30$ MeV, though the distribution of the unperturbed strength is very different in those two nuclei.

In Table II some calculated result of monopole modes is summarized. The difference between the two mean energies E_1 and E_3 becomes larger for a peak with a larger width (or for several peaks spreading over a larger energy region), since the quantity E_3 is obtained by heavily weighting the

TABLE II. Properties of monopole modes and the mean field. $\varepsilon_p^{\rm thr}(\varepsilon_n^{\rm thr})$ expresses the proton (neutron) threshold energy, while $\langle r^2\rangle$ denotes the HF ground-state expectation value of isoscalar radius squared. $\bar{E}_k$ is defined in Eq. (14), while K in Eq. (15).

Nucleus	$^{110}_{28}$Ni$_{82}$	$^{100}_{50}$Sn$_{50}$	$^{120}_{38}$Sr$_{82}$	$^{120}_{50}$Sn$_{70}$
$\varepsilon_p^{\rm thr}$ (MeV)	30.6	3.2	21.7	10.4
$\varepsilon_n^{\rm thr}$ (MeV)	0.8	17.0	4.4	8.3
$\langle r^2\rangle$(fm^2)	23.2	19.2	22.8	21.9
Isoscalar mode				
$\bar{E}_1$ (MeV)	10.5	18.1	13.6	15.8
$\bar{E}_3$ (MeV)	14.0	18.9	15.3	16.7
K (MeV)	61	151	101	131
Isovector mode				
$\bar{E}_1$ (MeV)	15.9	31.2	22.5	26.6
$\bar{E}_3$ (MeV)	27.1	35.3	30.6	31.4

higher-lying strength. Using $\bar{E}_1$, the calculated quantity

$$K=\bar{E}_1^2\,\frac{m\langle r^2\rangle}{\hbar^2} \tag{15}$$

is also given, which may be a measure of the incompressibility of the nuclei. Smaller K values obtained for nuclei with larger $(N-Z)/A$ values in Table II may come partly from the strong softening of the equation of state going from symmetric to asymmetric nuclear matter [16] and partly from the very low particle threshold in the neutron-drip-line nuclei. For reference, the excitation energy of isoscalar monopole GR observed in β-stable nuclei is approximately written as $76A^{-1/3}$ MeV for $A\approx 120$ (see, for example, Ref. [17]), which gives 16.4, 15.9, and 15.4 MeV for $A=100$, 110, and 120, respectively. There is some evidence for isovector monopole modes in experiments, however, the sum rule consumed by the observed modes is not yet well established. Thus, we may say that the frequency of the GR is not yet known even for β-stable nuclei. On the other hand, the hydrodynamical model by Bohr and Mottelson [10] predicts the frequency of the isovector monopole GR to be written as $170A^{-1/3}$ MeV, and other available models give more or less the same result.

The prominent contrast between the RPA monopole modes calculated for neutron-drip-line nuclei, β-stable nuclei, and proton-drip-line nuclei remains unchanged when other Skyrme interactions are used. However, the calculated distribution of the isoscalar monopole strength in a given nucleus, which is shown in Figs. 5(a)–5(d), is known to be sensitive to the incompressibility of the Skyrme interaction used [12]. For example, if the SIII interaction is used, of which the incompressibility for the nuclear matter is 356 MeV instead of (the more reasonable value of) 216 MeV as for the SkM* interaction, the calculated position of the RPA GR peak is shifted to a higher energy region by a few MeV. In addition, in the energy region just above the particle threshold the RPA isoscalar monopole strength is weaker than the unperturbed strength. This is principally due to the weakly repulsive nature of the p-h interaction derived from the SIII interaction at smaller distances.

In Fig. 6 the radial transition density of the RPA isoscalar monopole mode for $^{110}_{28}$Ni$_{82}$ and $^{100}_{50}$Sn$_{50}$ is shown at several energies. The radial dependence of $\rho_\lambda^{\rm tr}(r)$ is obtained from the imaginary part of $G_{\rm RPA}(\vec{r},\vec{r}';E_n)$ after the integration over one of the radial coordinates $\vec{r}'$, while the absolute magnitude is fixed using Eq. (11), of which the left-hand side is calculated from the energy integration of $S(E)$ in Eq. (5) over 1 MeV around E_n. The shape of the transition densities of $^{110}_{28}$Ni$_{82}$ at $E_x=11.75$ MeV or $^{100}_{50}$Sn$_{50}$ at $E_x=17.50$ MeV is that of a typical collective monopole mode, which changes the sign around the nuclear surface. Comparing those two collective transition densities we see that the transition density of the neutron-drip-line nucleus $^{110}_{28}$Ni$_{82}$ changes the sign at the place 0.7 fm outside that of $^{100}_{50}$Sn$_{50}$ and is extended to far outside of the nuclear radius. This appreciable amplitude of the transition density outside of the nuclear surface can affect strongly, for example, the reaction cross section by strongly absorbed particles. The transition density of $^{110}_{28}$Ni$_{82}$ at $E_x=23.25$ MeV represents a shape of a (proton) 1p-1h excitation, while the one at $E_x=5.0$ MeV is regarded as a typical shape coming from threshold phenomena.

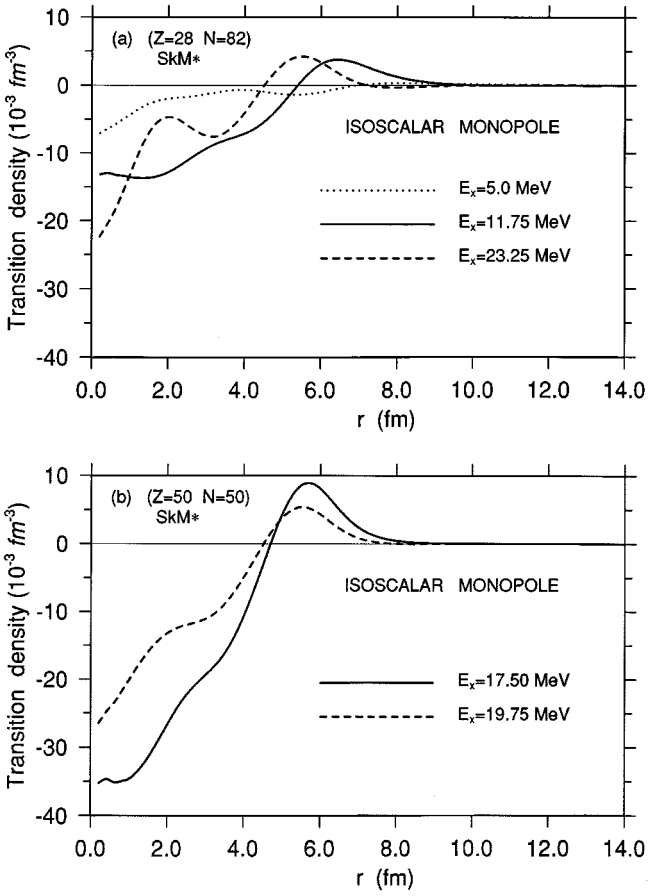

FIG. 6. Radial transition density, $\rho_\lambda^{\rm tr}(r)$ on the RHS of Eq. (12), of RPA isoscalar monopole mode at several energies as a function of radial coordinate: (a) $^{110}_{28}$Ni$_{82}$; (b) $^{100}_{50}$Sn$_{50}$. Transition densities plotted in Fig. 6(a) [6(b)] are those of the RPA isoscalar monopole modes at respective energies in Fig. 5(a) [5(b)].

B. Isovector dipole mode

In Fig. 7 the calculated strength function of the isovector dipole modes for $^{110}_{28}$Ni$_{82}$ and $^{100}_{50}$Sn$_{50}$ is shown. We note that

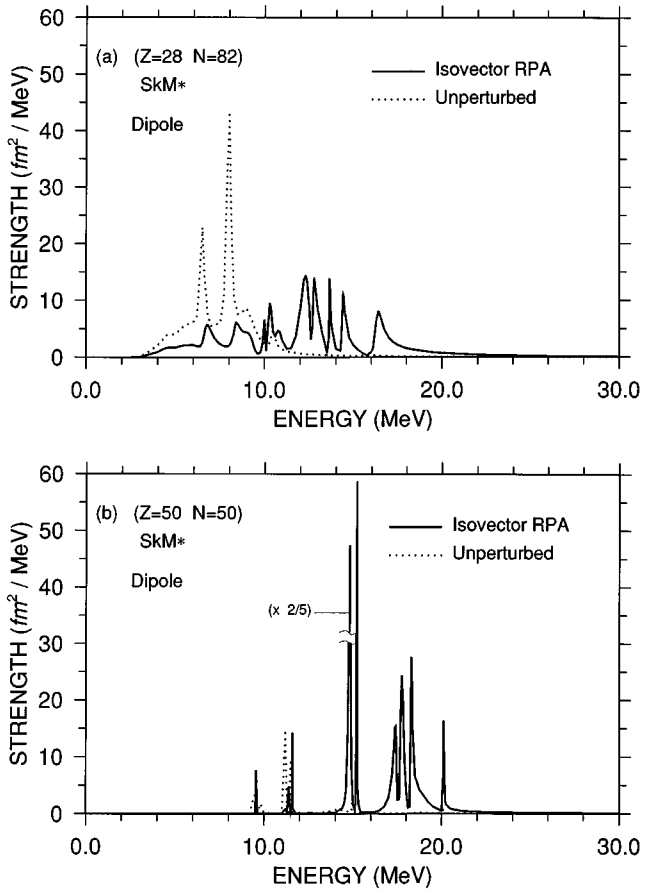

FIG. 7. The unperturbed strength function defined in Eq. (4) and the RPA strength function in Eq. (5) for isovector dipole mode as a function of excitation energy: (a) $^{110}_{28}\mathrm{Ni}_{82}$; (b) $^{100}_{50}\mathrm{Sn}_{50}$. In the region of 9.5–16 MeV several bound p-h excitations (proton configurations for ^{110}Ni and neutron configurations for ^{100}Sn) are present, which do not appear in the dotted lines of the figures. However, the RPA solution contains all strength. See the text.

in the present self-consistent RPA calculation the spurious center-of-mass motion is automatically separated out from the physically meaningful excitations [18]. In the harmonic oscillator model the dipole mode has only one unperturbed frequency ($=\hbar\omega_0$), just as the monopole mode has only one with $2\hbar\omega_0$. Because of the same reason as described for the unperturbed monopole strength in Sec. III A, in neutron-drip-line nuclei the calculated dipole strength of the unperturbed p-h excitations is spread over a large energy region. The dotted line in Fig. 7(a) contains only the neutron unperturbed strength, which has peaks in the energy region of 4–10.5 MeV. All proton unperturbed strengths (for $E<30$ MeV) come from bound p-h excitations and the major peaks are located in the region of 9.5–16 MeV. Thus, the major strength of the whole unperturbed p-h excitations in ^{110}Ni is spread over the region of 4–16 MeV. In contrast, in $^{100}_{50}\mathrm{Sn}_{50}$ the peaks of the dotted line in Fig. 7(b) express the proton unperturbed strength and are present in the region of 9–15 MeV. Almost all neutron strengths come from bound p-h excitations and the major peaks are localized in the region of 9.5–16 MeV, namely, in the same energy region of proton peaks.

TABLE III. Mean energies of isovector dipole modes and isoscalar quadrupole modes. E_k is defined in Eq. (14).

Nucleus	$^{110}_{28}\mathrm{Ni}_{82}$	$^{100}_{50}\mathrm{Sn}_{50}$
Isovector dipole mode		
$\bar{E}_1$ (MeV)	11.3	16.8
$\bar{E}_3$ (MeV)	14.8	17.8
Isoscalar quadrupole mode		
$\bar{E}_1$ (MeV)	4.6	9.9
$\bar{E}_3$ (MeV)	11.2	14.2

Due to the repulsive nature of the isovector interaction, the unperturbed dipole strength is shifted to a higher energy region when the RPA correlation is taken into account. Due to the very fragmented unperturbed p-h strength, the RPA dipole strength in $^{110}_{28}\mathrm{Ni}_{82}$ is seen to be very much fragmented in a large energy region and the center of the strength lies in an appreciably lower-energy region, compared with β-stable nuclei. In contrast, the distribution of the strength function in $^{100}_{50}\mathrm{Sn}_{50}$ is relatively similar to that in β-stable nuclei.

In Table III we list the calculated mean energies of isovector dipole modes. For reference, the frequency of isovector dipole GR observed in β-stable nuclei with $A>50$ is expressed as $79A^{-1/3}$ MeV (for example, see Ref. [10]), which gives 17.0 and 16.5 MeV for $A=100$ and 110, respectively.

C. Isoscalar quadrupole mode

In Fig. 8 the calculated transition strength of isoscalar quadrupole modes is shown. In the case of $^{110}_{28}\mathrm{Ni}_{82}$ shown in Fig. 8(a) an extremely strong sharp peak is obtained slightly above 1 MeV, which originates from the unperturbed neutron excitation $1h_{11/2}\rightarrow$(resonant)$2f_{7/2}$ at 2.2 MeV and collects the strength from higher-lying p-h excitations. The energy of the unperturbed 1p-1h 2^+ excitation, 2.2 MeV, which is unusually small for a doubly closed-shell nucleus, comes from the neutron shell structure unique in the neutron drip line [see Fig. 1(b)] and indicates that the neutron number $N=82$ is no longer a magic number. The bound proton p-h excitations $1f_{7/2}\rightarrow 1f_{5/2}$ and $1f_{7/2}\rightarrow 2p_{3/2}$ at 4.3 and 4.9 MeV, respectively, are responsible for the two RPA peaks at 4–5 MeV in Fig. 8(a). The GR is seen as one relatively broad peak centered around 11 MeV. Some unperturbed quadrupole strength of neutron excitations, in which the neutron holes are in the last-filled major shell, appears at very low excitation energies above the particle threshold, in a similar way as described in Sec. III A for the unperturbed monopole strength. However, in the case of the quadrupole operator those excitations carry only a fraction of the total strength, as observed in the dotted line of Fig. 8(a). The unperturbed bound proton p-h excitations for the quadrupole operator are found in the region of 20–30 MeV, corresponding to the proton excitations at 22–26 MeV in the case of monopole modes described in Sec. III A. However, in contrast to the case of monopole modes, they do couple strongly with the unperturbed excitations in the continuum by RPA correlations and, consequently, the p-h strength is shifted to the lower-energy region. This strong coupling comes from the surface-peaked shape of the interaction in the case of quad-

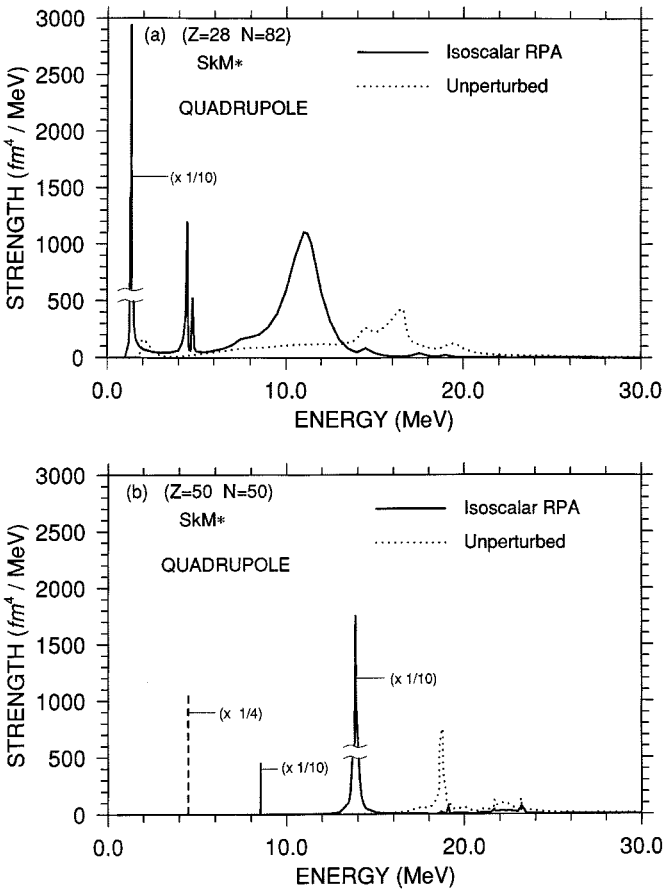

FIG. 8. The unperturbed strength function defined in Eq. (4) and the RPA strength function in Eq. (5) for isoscalar quadrupole mode as a function of excitation energy: (a) $^{110}_{28}\mathrm{Ni}_{82}$; (b) $^{100}_{50}\mathrm{Sn}_{50}$. In the region of both 4–9 MeV and 20–30 MeV several bound p-h excitations (proton configurations for ^{110}Ni and neutron configurations for ^{100}Sn) are present, which do not appear in the dotted lines of the figures. However, the RPA solution contains all strength. For the extremely sharp strong peak at 4.5 MeV in $^{100}_{50}\mathrm{Sn}_{50}$ the estimated $B(\lambda=2)$ value in units of fm^4 is shown in Fig. 8(b) by a vertical dashed line, instead of plotting the strength function. See the text for details.

rupole modes, which produces the strong coupling for almost all p-h excitations irrespective of the form factors.

In the case of $^{100}_{50}\mathrm{Sn}_{50}$ the RPA solution at 4.5 MeV lies above the particle (proton) threshold, 3.2 MeV. However, the peak has a very large height with an extremely narrow width. Therefore, instead of plotting the strength function, in Fig. 8(b) the estimated $B(\lambda=2)$ value for the peak is shown by a vertical dashed line in units of fm^4. The bound neutron p-h excitations, $1g_{9/2}\rightarrow 2d_{5/2}$ and $1g_{9/2}\rightarrow 1g_{7/2}$, are at 5.9 and 8.6 MeV, respectively, while the unperturbed proton excitations, $1g_{9/2}\rightarrow$(resonant)$2d_{5/2}$ and $1g_{9/2}\rightarrow$(resonant)$1g_{7/2}$, are at 5.7 and 8.3 MeV. It is seen that in this proton-drip-line nucleus ^{100}Sn the unperturbed $\Delta N_{sh}=0$ excitations as well as the $\Delta N_{sh}=2$ excitations have nearly the same energies for protons and neutrons. Consequently, the isoscalar quadrupole GR is obtained as a relatively narrow peak around 14 MeV, which is a slightly higher energy than that of the GR known in β-stable nuclei.

In Table III the calculated mean energies are listed. For reference, the excitation energy of the isoscalar quadrupole GR observed in β-stable nuclei is expressed as $58A^{-1/3}$ MeV, which gives 12.5 and 12.1 MeV for $A=100$ and 110, respectively.

The isoscalar quadrupole mode in a very light neutron-drip-line nucleus $^{28}_{8}\mathrm{O}_{20}$ was estimated in Ref. [19] using HF plus RPA. However, since the particle continuum was not treated in a proper way, the very interesting feature coming from the very small threshold energy in neutron-drip-line nuclei, which is discussed in our present work, did not seem to be properly pinned down in Ref. [19].

IV. CONCLUSIONS AND DISCUSSIONS

We have studied the structure of single-particle levels of both neutron-drip-line and proton-drip-line nuclei solving the spherical HF equation and further estimating the one-particle resonant states in the HF potential. It is found that for neutron orbitals with $\varepsilon\gtrsim -1.5$ MeV the one-particle levels with lower angular momenta are appreciably pushed down relative to those with higher angular momenta, as the neutron drip line approaches. The lowering of those neutron one-particle levels is due to the neutron potential with very diffused surface, since the orbitals with lower angular momenta and more radial nodes are energetically favored in the diffused potential. A similar, but much less pronounced, variation of the shell structure is observed in some proton one-particle resonant energies, as we approach the proton drip line.

Next, the unperturbed monopole strength is studied by the Green's function method. We have found that in neutron-drip-line nuclei an appreciable amount of the neutron strength lies in the region of drastically low excitation energy compared with β-stable nuclei. These strengths come from the configurations in which the holes are in the major shell just below the Fermi levels. The energies at which the strengths of those configurations reach the maximum are not related to the resonance energies of the one-particle motion of neutrons. On the other hand, the energies of the proton p-h excitations are slightly higher than those in β-stable nuclei. Consequently, the essential part of the whole unperturbed p-h strength is fragmented over a very large energy region; for example, 6–26 MeV in the case of $^{110}_{28}\mathrm{Ni}_{82}$. Thus, the properties of collective modes in neutron-drip-line nuclei can be very different from those in β-stable nuclei. In contrast, in proton-drip-line nuclei the energies of unperturbed proton excitations are pretty similar to those of neutron p-h excitations.

Solving the RPA equation with the Green's function method, the isoscalar monopole GR in neutron-drip-line nuclei is found to lie in a very low frequency region and have a large width, compared with the case of β-stable nuclei. In contrast, the isoscalar monopole GR in proton-drip-line nuclei is relatively similar to that in β-stable nuclei, though the frequency is slightly higher.

The RPA strength of the isovector monopole mode in neutron-drip-line nuclei has an extremely fragmented distribution, which consists of approximately two parts; the lower-lying part unique in neutron-drip-line nuclei and the higher-lying peak which is similar to the GR known in β-stable nuclei. In contrast, the RPA isovector monopole strength of proton-drip-line nuclei has only one GR peak similar to the

one in β-stable nuclei, though some RPA strength is found in a lower frequency region.

The difference of the distribution of the isovector dipole strength between neutron-drip-line nuclei and proton-drip-line nuclei is analogous to that in the case of the isovector monopole strength. The RPA dipole strength in $^{110}_{28}\mathrm{Ni}_{82}$ is fragmented over a large energy region, of which the center lies appreciably lower than that of β-stable nuclei, while the distribution of the RPA dipole strength in $^{100}_{50}\mathrm{Sn}_{50}$ is relatively similar to that of β-stable nuclei.

In the doubly magic nucleus $^{110}_{28}\mathrm{Ni}_{82}$ we have obtained a strongly collective 2^+ state slightly above 1 MeV, which originates from the unperturbed neutron excitation, $1h_{11/2}\rightarrow$(resonant)$2f_{7/2}$, lying at so low as 2.2 MeV. The isoscalar quadrupole GR has a broad width centered around 11 MeV, which is appreciably lower than the frequency of the GR known in β-stable nuclei. In the proton-drip-line nucleus $^{100}_{50}\mathrm{Sn}_{50}$ the unperturbed quadrupole p-h excitations with $\Delta N_{sh}=0$ as well as those with $\Delta N_{sh}=2$ have similar frequencies for protons and neutrons. Consequently, the isoscalar quadrupole GR appears as one peak, of which the frequency is slightly higher than that in β-stable nuclei, with a relatively narrow width.

ACKNOWLEDGMENTS

The authors would like to express their sincere thanks to Professor Ben Mottelson for fruitful discussions. One of the authors (X.Z.Z.) is grateful to Crafoordska Stiftelsen for a financial support, while the other (H.S.) to Japan Society for the Promotion of Science (JSPS).

[1] For example, see, C. Detraz and D. C. Vieira, Annu. Rev. Nucl. Part. Sci. **39**, 407 (1989); I. Tanihata, in *Treatise on Heavy-Ion Science*, edited by D. A. Bromley (Plenum, New York, 1989), Vol. 8, pp. 443–514; E. Roeckl, Rep. Prog. Phys. **55**, 1661 (1992); A. C. Mueller and B. M. Sherrill, Annu. Rev. Nucl. Part. Sci. **43**, 529 (1993).

[2] I. Tanihata, H. Hamagaki, O. Hashimoto, Y. Shida, N. Yoshikawa, K. Sugimoto, O. Yamakawa, T. Kobayashi, and Y. Takahashi, Phys. Rev. Lett. **55**, 2676 (1985); P. G. Hansen and B. Jonson, Europhys. Lett. **4**, 409 (1987).

[3] D. Hirata, H. Toki, T. Watabe, I. Tanihata, and B. V. Carlson, Phys. Rev. C **44**, 1467 (1991).

[4] J. Dobaczewski, I. Hamamoto, W. Nazarewicz, and J. A. Sheikh, Phys. Rev. Lett. **72**, 981 (1994).

[5] W. D. Myers, W. J. Swiatecki, and C. S. Wang, Nucl. Phys. A **436**, 185 (1985).

[6] A. Krasznahorkay *et al.*, Phys. Rev. Lett. **66**, 1287 (1991); I. Tanihata, D. Hirata, T. Kobayashi, S. Shimoura, K. Sugimoto, and H. Toki, Phys. Lett. B **289**, 261 (1992).

[7] I. Hamamoto and X. Z. Zhang, Phys. Rev. C **52**, R 2326 (1995).

[8] H. Sagawa, B. A. Brown, and H. Esbensen, Phys. Lett. B **309**, 1 (1993).

[9] S. Shlomo and G. F. Bertsch, Nucl. Phys. A **243**, 507 (1975).

[10] A. Bohr and B. R. Mottelson, *Nuclear Structure*, Vol. II (Benjamin, New York, 1975).

[11] B. Chen, J. Dobaczewski, K.-L. Kratz, K. Langanke, B. Pfeiffer, F.-K. Thielemann, and P. Vogel, Phys. Lett. B **355**, 37 (1995), and references quoted therein.

[12] N. Van Giai and H. Sagawa, Nucl. Phys. A **371**, 1 (1981).

[13] J. M. Blatt and V. F. Weisskopf, *Theoretical Nuclear Physics* (Wiley, New York, 1952), Chap. VIII.

[14] H. Sagawa, Nucl. Phys. A **538**, 619c (1992).

[15] H. Sagawa, N. Van Giai, N. Takigawa, M. Ishihara, and K. Yazaki, Z. Phys. A **351**, 385 (1995).

[16] I. Bombaci and U. Lombardo, Phys. Rev. C **44**, 1892 (1991) and references quoted therein.

[17] M. M. Sharma, W. T. A. Borghols, S. Brandenburg, S. Crona, A. van der Woude, and M. N. Harakeh, Phys. Rev. C **38**, 2562 (1988).

[18] D. J. Thouless, Nucl. Phys. **21**, 225 (1960).

[19] T. Otsuka, A. Muta, M. Yokoyama, N. Fukunishi, and T. Suzuki, Nucl. Phys. A **588**, 113c (1995).